fluids

MDPI

Article

CFD Analysis of Hydrodynamic Loads on Jack-Up Platforms Using Buoyancy-Modified k-ω SST Turbulence Model

Nu Rhahida Arini [1,*], Gilang Muhammad [1], Eko Charnius Ilman [2], Teguh Hady Ariwibowo [1], Mohamed Moshrefi-Torbati [3] and Deni Saputra [1]

[1] Power Plant Engineering Program, Department of Mechanical Engineering and Energy, Politeknik Elektronika Negeri Surabaya, Surabaya 60111, Indonesia; gilang25111998@outlook.co.id (G.M.); teguhhady@pens.ac.id (T.H.A.); denisaputra1102@pg.student.pens.ac.id (D.S.)
[2] Ocean Engineering Program, Faculty of Civil and Environmental Engineering, Institut Teknologi Bandung, Bandung 40132, Indonesia; eko.ilman@itb.ac.id
[3] Department of Mechanical Engineering, Faculty of Engineering and Physical Sciences, School of Engineering, University of Southampton, Highfield Campus, Southampton SO17 1BJ, UK; m.m.torbati@soton.ac.uk
* Correspondence: arini@pens.ac.id

Abstract: The offshore jack-up production platform operates in extreme and unpredictable marine environments. Therefore, its structural strength must be designed to withstand harsh conditions, particularly hydrodynamic loads from waves and ocean currents. This study aims to numerically analyze the interaction of marine hydrodynamic forces with a jack-up production platform using OpenFOAM v1606, a Computational Fluid Dynamics (CFD) software. Specifically, the research evaluates a buoyancy-modified k−ω SST turbulence model based on the Standard Gradient Diffusion Hypothesis (SGDH) on a 3D jack-up platform model. The analysis is conducted using a Stokes 5th-order wave model within the waves2Foam toolbox, considering four variations in wave height and period. The results demonstrate that the modified turbulence model provides more accurate predictions. Additionally, they reveal that the forces acting on the platform's walls are directly proportional to wave height and period, with the highest recorded load reaching 4000 N in Case A, where the wave height and period are 5.4 m and 5.9 s, respectively. Furthermore, it is observed that most of the forces exerted on the platform hull are vertical, primarily due to the negative pressure on the platform's bottom side.

Keywords: Computational Fluid Dynamic; jack-up production platform; OpenFOAM; k-ω SST

Academic Editors: Markus Klein, Hao Chen and Deping Cao

Received: 25 February 2025
Revised: 29 March 2025
Accepted: 1 April 2025
Published: 4 April 2025

Citation: Arini, N.R.; Muhammad, G.; Ilman, E.C.; Ariwibowo, T.H.; Moshrefi-Torbati, M.; Saputra, D. CFD Analysis of Hydrodynamic Loads on Jack-Up Platforms Using Buoyancy-Modified k-ω SST Turbulence Model. *Fluids* **2025**, *10*, 96. https://doi.org/10.3390/fluids10040096

1. Introduction

The global demand for energy is steadily increasing, making petroleum and natural gas vital resources. These energy sources serve as raw materials for oil, fuel gas, and various chemical products, powering homes, industries, and economies. As a result, they remain essential contributors to the world's energy supply. A statistical analysis indicates a significant rise in oil consumption, increasing from 1.4 million barrels per day (b/d) in 2018 to 2.9 million b/d in 2022. Likewise, natural gas consumption has surged from 195 billion cubic meters in 2018 to 542 billion cubic meters in 2022 [1,2]. These data highlight the critical role of petroleum and natural gas in meeting the world's growing energy needs.

The extraction of oil and natural gas relies on exploiting proven reservoirs, a process facilitated by jack-up production platforms. These platforms are specifically designed to drill into underground reservoirs for resource extraction and are strategically positioned

based on reservoir location. Jack-up platforms fall into three main categories: fixed structures, typically used at depths of 100–200 m (328–656 feet); floating structures, operating at depths of around 200 m (656 feet); and compliant structures, designed for depths exceeding 1000 m (3280 feet) [3]. Oil wells can be located onshore or offshore, with offshore drilling requiring additional infrastructure to support drilling and production operations. Each type of the jack-up platform is built for specific depth conditions, enabling offshore platforms to function in extreme and unpredictable environments. As a result, their structural integrity must withstand harsh marine conditions, particularly hydrodynamic loads from waves and ocean currents [3].

The structural parts of offshore platforms with a high level of vulnerability are the support leg and hull/deck structures. This vulnerability stems from the exposure to loading, which is induced by waves and ocean currents, known as hydrodynamic loads. The hydrodynamic loads exert the most significant impact on offshore structures [4,5]. A numerical model can represent an offshore production platform with a certain degree of accuracy when subjected to actual marine hydrodynamic loads. This modeling enables the estimation of the magnitude of the load and the resulting pressure on the production platform. There are numerous studies on hydrodynamic loads applied to offshore production platforms through numerical methods such as the studies by Kagita et al., Luo-Theilen and Rung, Ye et al., and Tang et al.; these studies contribute valuable insights into understanding how different load conditions, including the varied characteristics of load waves, impact the platform through numerical methods [6–9].

Extensive experimental and theoretical studies have been conducted to better understand wave dynamics on offshore structures. However, experimental research on offshore structures is often expensive and challenging due to the complexity of ocean environment modeling and instrumentation [10,11]. As an alternative, scaled models can be used for evaluations. A numerical model, particularly the Computational Fluid Dynamics (CFD) method, serves as a reliable predictive tool. CFD has the capability to model free-surface flow under multiphase wave generation conditions. In this study, OpenFOAM, an open-source CFD tool widely used in engineering, is employed to provide detailed and accurate predictions of fluid flow phenomena. By utilizing CFD, research can be conducted cost-effectively and efficiently, as demonstrated by previous studies from Wu, Zhou et al., Jiang et al., and Elhanafi et al. [12–15]. However, developing CFD models and configuring hydrodynamic load setups remain as the areas of ongoing research. A key challenge is accurately predicting fluid behavior at the free surface in wave generation models. This study aims to numerically investigate CFD configurations using a modified k$-\omega$ SST turbulence model to predict hydrodynamic loads on a jack-up platform.

Extensive research has been conducted on wave dynamics and their interactions with offshore structures. Elhanafi et al. numerically and experimentally investigated the effects of wave period, wave height, and power take-off (PTO) attenuation using the Reynolds-Averaged Navier–Stokes (RANS) equations coupled with the surface-capturing Volume of Fluid (VOF) scheme to predict wave-generated forces [15]. Their study found that the horizontal wave force acting on an Oscillating Water Column (OWC) device is consistently greater than the vertical force. Additionally, an increasing wave height amplifies nonlinear effects, particularly on vertical force measurements. Similarly, other studies utilizing the RANS equations with the VOF scheme have investigated the various aspects of wave interactions, including spatial distribution, wave breaking, and wave transformation [16–18]. Despite variations in research focus, both experimental studies and numerical simulations consistently produce highly relevant and accurate results, reinforcing the reliability of these modeling approaches.

Free surface models in fluid dynamics cannot be overstated, especially in research focused on wave behavior. The model plays a crucial role in understanding and simulating the dynamic wave, offering researchers valuable data to analyze the waves. In modeling free surfaces, various methods can be used. The Level Set Method (LSM) is one of the numerical methods based upon representing an interface of surfaces or shapes. Numerous studies have utilized this method in their research, as demonstrated by Aggarwal et al., Chella, Bihs, and Myrhaug, Leftheoretis et al., Wang et al., and Frantzis, Grigoriadis, and Dimas [19–23]. These studies were conducted to investigate the different parameters (e.g., density, pressure and kinematic, velocity, multi-directional wave, and wave breaking) and their different platforms to use these methods (e.g., monopile, Hybrid parallel, flat bottom tank, and single row vertical pile).

Not only do numerical methods impact free surface modeling, but the free surface elevations in numerical results must also be validated against an ideal wave profile. This validation is typically performed using the Stokes wave theory, particularly the fifth-order Stokes wave, which has been widely used in studies on dynamic wave behavior due to its well-documented accuracy in representing free surface elevations [24]. By comparing numerical results with the ideal wave profile generated by the fifth-order Stokes wave theory, the reliability of free surface elevation predictions can be effectively assessed. Dong et al. conducted valuable research on Stokes wave comparisons, demonstrating that fifth-order Stokes waves improve accuracy in energy density values, extending to the tenth-order compared to previous models [25]. Their study found that as nonlinearity increased, kinetic energy surpassed potential energy, disrupting the traditional relationship between energy and wave height. Additionally, greater wave nonlinearity led to an uneven energy distribution, with rising crest energy dominating the wave profile. Overall, this research provides valuable insights into the energy dynamics and nonlinear characteristics of fifth-order Stokes waves, further reinforcing their role in wave modeling and validation.

In free surface research involving wave formation, a common issue is the gradual weakening of waves over the extended simulation periods. This phenomenon occurs due to the excessive formation of turbulent kinetic energy near the water's surface. Devolder, Ruwoens, and Troch addressed this problem by modifying the k-ω SST turbulence model, incorporating density and buoyancy terms into the turbulence equations [26]. Modifying the turbulence model was necessary to mitigate the effects of excessive turbulence levels, which significantly impact the wave profile. This issue was effectively resolved by integrating the buoyancy equation—based on the Standard Gradient Diffusion Hypothesis (SGDH)—into the kinetic turbulence energy (k) equation. A wave simulation experiment on a monopile structure was conducted using the OpenFOAM CFD tool, employing the IH-FOAM wave generator and an absorber toolbox. The results demonstrated that in an empty wave flume, excessive turbulence levels, particularly in high-steepness waves, caused deviations from the expected fifth-order Stokes wave profile. This research highlights the importance of turbulence model adjustments in ensuring accurate wave simulations.

In a previous study, Devolder, Ruwoens, and Troch successfully applied the modified k-ω SST turbulence model to analyze wave loads on a simple monopile structure [26]. Similarly, Huo et al. investigated slamming impact using a modified k-ω SST model, achieving effective wave condition generation for Cylindrical Floating Production Storage and Offloading (CFPSO) systems [27]. While both studies demonstrated the effectiveness of the modified k-ω SST model, research on this approach remains limited, particularly in cases involving complex offshore structures. To address this gap, the present study focuses on CFD modeling of an offshore jack-up production platform, simulating ocean hydrodynamic loads using OpenFOAM. The simulation conditions are designed to reflect the real environmental factors of the Madura Strait. Four test cases will be conducted,

each with different wave heights and wave periods, to assess the impact of hydrodynamic loads on the jack-up platform structure. By applying the modified k-ω SST model to a more complex geometry, this study aims to evaluate the model's ability to capture wave breaking phenomena. The data obtained will be crucial for further structural strength analysis, particularly in understanding how wave breaking at varying heights influences the platform's stability and performance.

2. Jack-Up Platform Configuration

The hydrodynamic load of sea waves on the hull section of a jack-up production platform is estimated in this study. To simplify the analysis, the hull geometry is considered without the supporting legs. Since the supporting structures are relatively small compared to the hull, their interaction with waves is assumed to be negligible in the simulation. Therefore, the study primarily focuses on the hull's response to hydrodynamic loads.

2.1. Jack-Up Platform Geometric and Domain

The jack-up production platform has a substantial structure, measuring 53.65 m × 40.21 m × 4.93 m. For a detailed view of its geometry, refer to Figure 1, which provides a visual representation of the platform. This visualization assumes the absence of shoreline effects and external loads on the hull, allowing for a clearer focus on the structural design.

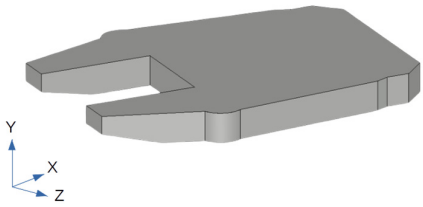

Figure 1. Jack-up production platform hull geometry.

Figure 2 illustrates the computational domain, spanning a length of 295 m, a width of 100 m, and a height of 100 m. The focus within this domain is the hull geometry, strategically positioned at its core, where the hull geometry domain is in the center of the computational domain. In the following research, the waves2Foam toolbox is used to generate waves and absorb waves as introduced by Jacobsen, Fuhrman, and Fredsøe [28]. The toolbox is designed for simulating wave generation, propagation, and interaction with structures. It is widely used in coastal, offshore, and naval engineering applications. This toolbox incorporates relaxation zones to dissipate reflected waves, minimizing unwanted reflections from boundaries, including the outlet [29]. This ensures realistic offshore and coastal simulations.

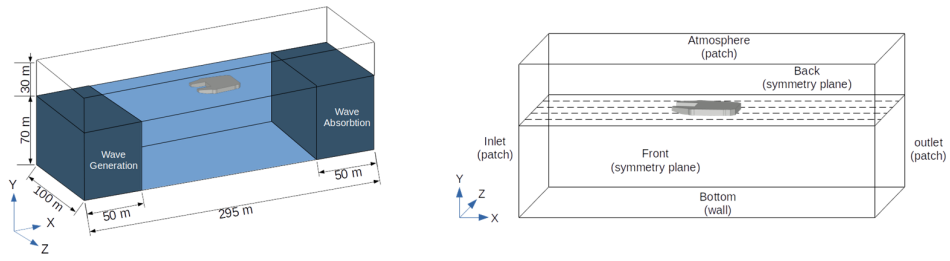

(a) (b)

Figure 2. (**a**) Computation domain. (**b**) Boundary condition.

The computational domain is designed with a wave generation zone and a wave relaxation zone, positioned at both ends of the 50 m-long domain. The domain length is

based on one wavelength (λ_L) calculated using the formula $\lambda_L = \frac{2\pi}{k}$ where k is wave number determined through iterative calculations in the waves2Foam solver. This approach, previously implemented by Brown et al. [30], effectively prevents wave reflection and interference, ensuring smooth wave propagation along the x-axis. Additionally, the water depth for this study is set at 70 m, aligning with the specified research parameters.

The position of the jack-up production platform geometry is adjusted as the bottom of the production platform is at half the wave height of the still water level (SWL) as in Figure 3, which represents the extreme operating conditions that may occur.

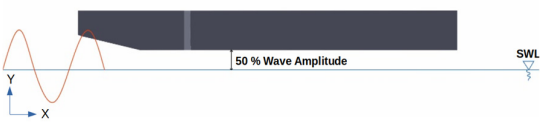

Figure 3. Jack-up production platform hull position.

2.2. Meshing and Boundary Condition

The computational domain is divided into distinct regions for water and air, each assigned a specific boundary conditions. The inlet, outlet, and atmosphere are defined as patch boundary conditions, while symmetrical conditions are applied to the front and back. For turbulence parameters, such as turbulence kinetic energy and turbulence dissipation, outflow conditions are assigned, with specified inflow conditions applied in return flow scenarios. Turbulence viscosity is configured to allow fluid to flow out of the domain. The bottom surface and the jack-up production platform are treated as fixed-wall boundary conditions, reflecting the stationary position of the platform. For a visual representation of the boundary condition scheme, refer to Figure 2b.

A 3D structured mesh was generated using cfMesh, specifically designed for simulating a single wave surface. The mesh consists of 18 cells along the vertical axis and 63 cells along the horizontal axis, following the methodology of Islam and Guedes Soares [31]. This setup results in a total of 1,957,004 cells for the wave run-up simulation on the monopile structure, as illustrated in Figure 4a. Meanwhile, the jack-up platform mesh topology consists of 1,540,316 cells, as shown in Figure 4b. To enhance accuracy, the mesh near the wall region is refined to capture boundary layer effects more precisely. Additionally, a wall function is applied to the surface of the jack-up production platform, ensuring turbulent viscosity and kinetic energy adaptation to the surrounding flow conditions.

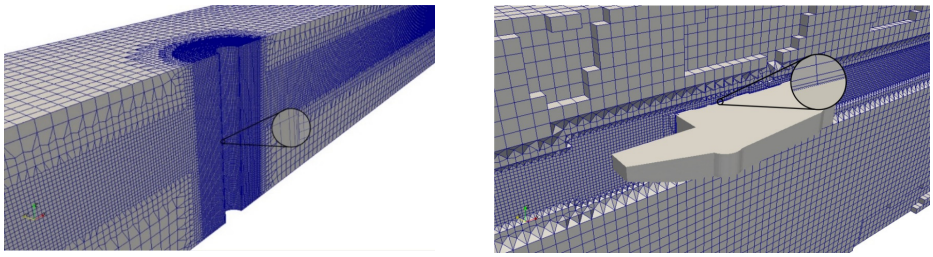

(**a**) (**b**)

Figure 4. (**a**) Mesh topology on monopile structure. (**b**) Mesh topology on jack-up platform.

To optimize computational efficiency, the geometric dimensions of the computational domain are scaled down using a 1:100 ratio. In most hydrodynamic cases, where the object is too large to be fully modeled in CFD, significant scaling down is common. However, such scaling is considered valid only if it adheres to dimensionless similarity principles. In hydrodynamic problems, particularly those involving free-surface flows—such as waves, ship hydrodynamics, and offshore structures like jack-up platforms—the Froude number

(Fr) is generally preferred over the Reynolds number (Re) because it governs gravity-driven effects in the system. Free-surface deformations, including wave breaking, wave reflection, and diffraction, are primarily influenced by gravity, making Fr the dominant parameter. In contrast, Re is more relevant in cases such as turbulent boundary layer analysis, where viscosity plays a key role.

The Froude scaling to the wave test case parameters is outlined in Table 1. The test cases were carefully selected to analyze the interaction between wave height and the platform's contact points, which frequently occur under real conditions and significantly impact the platform's stability and structural response.

- Case B serves as the reference case.
- Case A explores conditions with a higher wave height and longer wave periods compared to Case B.
- Case C examines scenarios with a lower wave height and shorter wave periods than Case B.
- Case D investigates the impact of varying wave heights while maintaining a constant wave period.

Table 1. Wave test case parameters.

Case	Wave Height (m)	Wave Periods (s)
A	5.4	5.9
B	4.6	5.5
C	4	5.1
D	3.7	5.5

3. Numerical Method

The simulation setup for this paper uses the finite volume method, the time scheme using Euler Implicit time discretization, and the maximum Courant number is set to 0.25.

3.1. Governing Equation

The Navier–Stokes equations are fundamental to fluid dynamics, describing the conservation of momentum in fluid flow. This equation and the mass conservation equation and can be written as follows [26]:

$$\frac{\partial u_i}{\partial x_i} = 0 \tag{1}$$

The momentum conservation equation can be described as follows:

$$\frac{\partial \rho u_i}{\partial t} + \frac{\partial \rho u_j u_i}{\partial x_j} - \frac{\partial}{\partial x_j}\left[\mu_{eff}\frac{\partial \rho u_j}{\partial x_j}\right] = -\frac{\partial p^*}{\partial t} + F_{b,i} + f_{\sigma,i} \tag{2}$$

where t is the time, u is the fluid velocity (i and j are the unit vectors), ρ is the density of the fluid, μ_{eff} is the effective dynamic viscosity, p* is the pressure over the hydrostatic, F_b is an external force, and f_σ is the surface tension tensor term.

3.2. Volume of Fluid

The interface between the water surface and the air is obtained from the VoF method. The VoF method is based on the volume fraction which is 0 for air-filled cells, 1 for water-

filled cells, and between 0 and 1 for water-air interface cells. The volume fraction is solved using the advection as in Equation (3) [32]:

$$\frac{\partial \alpha}{\partial t} + \nabla .\mathrm{u}\alpha + \nabla .u_r\alpha(1-\alpha) = 0 \tag{3}$$

In VOF simulations, forces such as gravity and surface tension act at the interface between phases. The phase fraction, α, takes values within the range $1 < \alpha < 10$ and is only active near the interface. Its strength is determined by the relative velocity, u_r, where $u_r = 1$. If values greater than 1 are used, the compression between the interfaces increases. The effective density and dynamic viscosity μ_{eff} of the fluid are calculated based on the volume fraction α.

$$\rho = \alpha\rho_{water} + (1-\alpha)\rho_{air} \tag{4}$$

$$\mu_{eff} = \alpha\mu_{water} + (1-\alpha)\mu_{air} + \rho v_t \tag{5}$$

where the value of ρv_t is the turbulent dynamic viscosity value.

3.3. Froude Scaling

Froude equation is usually used in fluid flow modeling on free surface flow, especially if the frictional force is neglected and the occurrence of high turbulence phenomena [33]. Froude similarity requires identical Froude number values between the model and the prototype. For example, the following scale ratio is generated from the basic assumptions of the Froude model, which assumes an equal Froude number between the model and the prototype.

$$\frac{V_m}{\sqrt{gL_m}} = \frac{V_p}{\sqrt{gL_p}} \tag{6}$$

The size of the acceleration due to gravity is not scaled, and the geometric size scale is $L_p = \lambda L_m$, so that $V_m/(L_m)0.5 = V_p/(\lambda L_m)0.5$ and the ratio scale is $\lambda^{0.5}$. Generally, higher speeds are required for the model. More details for wave modeling are listed in Table 2.

Table 2. Scale factor for various variables.

Variable	Unit	Scale Factor
Length	m	λ
Wave Height	m	λ
Wave Length	m	λ
Wave Period	s	$\lambda^{0.5}$
Force	N	λ^3
Mass	Kg	λ^3
Pressure	Pa	λ
Moment	Nm	λ^4

3.4. Turbulence Model

Turbulent model equations are required to model the phenomenon of turbulence flow. The k-ω SST turbulent model is a turbulent model that is widely used in Computational Fluid Dynamics (CFD). The model simulates turbulent flow characteristics in the case of marine hydrodynamic loads as suggested by Keser [34]. The k-ω SST turbulent model, which is applied in the hydrodynamic load cases, is written in Equations (7)–(17). The transport equation for the turbulent kinetic energy (k) and dissipation rate (ω) in turbulence modeling is written in Equations (7) and (8).

Transport equation is as follows:

$$\frac{\partial}{\partial t}(\rho k) + \frac{\partial}{\partial x_i}(\rho k u_i) = \frac{\partial}{\partial x_j}\left[\Gamma_k \frac{\partial k}{\partial x_j}\right] + G_k - Y_k \tag{7}$$

$$\frac{\partial}{\partial t}(\rho \omega) + \frac{\partial}{\partial x_i}(\rho \omega u_i) = \frac{\partial}{\partial x_j}\left[\Gamma_\omega \frac{\partial \omega}{\partial x_j}\right] + G_\omega - Y_\omega + D_\omega \tag{8}$$

Effective diffusivity is as follows:

$$\Gamma_k = \mu + \frac{\mu_t}{\sigma_k},\ \Gamma_\omega = \mu + \frac{\mu_t}{\sigma_\omega},\ \mu_t = \frac{\rho k}{\omega}\frac{1}{max\left[\frac{1}{\alpha^*}, \frac{SF_2}{\alpha_1 \omega}\right]} \tag{9}$$

where S is the strain rate magnitude. And σ_k and σ_ω are given by the following equation:

$$\sigma_k = \frac{1}{F_1/\sigma_{k,1} + (1-F_1)/\sigma_{k,2}},\ \sigma_\omega = \frac{1}{F_1/\sigma_{\omega,1} + (1-F_1)/\sigma_{\omega,2}} \tag{10}$$

Turbulence production is as follows:

$$G_\omega = \frac{\alpha \alpha^*}{k} G_k,\ \alpha_\infty = F_1 \alpha_{\infty,1} + (1-F_1)\alpha_{\infty,2} \tag{11}$$

For the transport equations, turbulence dissipation is as follows:

$$Y_k = \rho \beta^* k \omega,\ \ Y_\omega = \rho \beta \omega^2,\ \beta_i = F_1 \beta_{i,1} + (1-F_1)\beta_{i,2} \tag{12}$$

The following model adopts the default value below:

$$\sigma_{k,1} = 1.176 \qquad \sigma_{k,2} = 2.0 \qquad \sigma_{\omega,1} = 1.0 \qquad \sigma_{\omega,2} = 1.168$$
$$\alpha_1 = 0.31 \qquad \beta_{i,1} = 0.075 \qquad \beta_{i,2} = 0.0828$$

$$\frac{\partial k}{\partial t} + \nabla.(\overline{u}k) - k\nabla.\overline{u} - \nabla.((\alpha_k v_t + v)\nabla k) = min(G,\ c_1 \beta^* k \omega) - \beta^* k \omega \tag{13}$$

$$\frac{\partial \omega}{\partial t} + \nabla.(\overline{u}\omega) - \omega\nabla.\overline{u} - \nabla.((\alpha_\omega v_t + v)\nabla \omega) = \gamma min\left[S_2, \frac{c_1}{a_1}\beta^* \omega max\left(a_1\omega,\ b_1 F_{23}\sqrt{S_2}\right)\right] - \beta\omega^2 + (1-F_1)CD_{k\omega} \tag{14}$$

And the viscosity of turbulence determined by Equation (15):

$$v_t = \frac{a_1 k}{max\left[a_1\omega, b_1 F_{23}\sqrt{2}\left|\frac{1}{2}\left(\nabla\overline{u} + (\nabla\overline{u})^T\right)\right|\right]} \tag{15}$$

The values G and S_2 are found using the following equation:

$$G = v_t S_2 \tag{16}$$

$$S_2 = 2\left|\frac{1}{2}\left(\nabla\overline{u} + (\nabla\overline{u})^T\right)\right|^2 \tag{17}$$

In the subsequent equation, the parameters (β) = 0.09, (a_1) = 0.31, (b_1) = 1, and (c_1) = 10 are established. However, when dealing with a free surface scenario, the utilization of the k-ω SST turbulent model yields significant wave damping, as evidenced by the reduction in incoming wave height. This occurrence is affected by the escalated turbulent viscosity within the surface vicinity, driven by the heightened formation rate of turbulent kinetic energy. In the research conducted by Devolder [35], an augmentation was made by introducing the k-ω SST

turbulence equation, denoted as SGDH, aimed at mitigating turbulent intensity in the water surface domain, thereby yielding Equation (18):

$$G_b = -\frac{v_t}{\sigma_t}\frac{\partial \rho}{\partial x_j}g_j \tag{18}$$

Additionally, a correction factor for the added omega part, as proposed by Kumar and Dewan [36], has been incorporated to address the issue of excessive turbulence inherent in multiphase flow regime affected by SGDH.

$$G_{b\omega} = \frac{1}{v_t}[(\gamma_1 + 1)C_3.max(G_b, 0) - G_b] \tag{19}$$

where (γ_1) = 5/9 dan (C_3) = 1. Furthermore, the inclusion of density and buoyant force terms in the transport equation stems from the variation in density values within the surface interface between water and air [37]. As a result, the modified equation for the k-ω SST turbulence model can be observed in the following expression:

$$\frac{\partial \rho k}{\partial t} + \nabla.(\rho \overline{u} k) - k\nabla.\rho\overline{u} - \nabla.(\rho(\alpha_k v_t + v)\nabla k) = min(\rho G,\ c_1\beta^*\rho k\omega) + G_b - \rho\beta^* k\omega \tag{20}$$

$$\frac{\partial \rho\omega}{\partial t} + \nabla.(\rho\overline{u}\omega) - \omega\nabla.\rho\overline{u} - \nabla.(\rho(\alpha_\omega v_t + v)\nabla\omega) = \rho\gamma min\left[S_2, \frac{c_1}{a_1}\beta^*\omega max\left(a_1\omega,\ b_1F_{23}\sqrt{S_2}\right)\right] + G_{b\omega} - \rho\beta\omega^2 + \rho(1 - F_1)CD_{k\omega} \tag{21}$$

4. Results and Discussion

4.1. Verification

Verification and validation are essential to ensuring the accuracy and reliability of simulation configurations. In this study, a comprehensive verification process was conducted using a simulation framework developed by Devolder, Rauwoens, and Troch [26]. The framework is based on Stokes' fifth-order wave theory and employs identical boundary conditions and domain configurations. The results indicated that the kinematic viscosity remained nearly laminar, validating the correctness of the simulation setup. The verification process involved analyzing the hydrodynamic forces acting on a monopile structure, which were then compared to theoretical estimates. The presence of the monopile had a significant impact on wave dynamics, particularly during wave breaking phenomena, highlighting the importance of the structural interactions in offshore environments.

The computational domain used in this study is illustrated in Figure 5a, which shows that the wave generation and wave absorption zones have equal lengths to minimize wave reflection. The domain is a three-dimensional space with dimensions of 20 m in length, 0.75 m in width, and 0.8 m in height. The monopile structure, which plays a central role in this analysis, has a diameter of 0.12 m, as depicted in Figure 5b. Jasak et al., Liu et al., and Chen et al. conducted numerical evaluations of wave loads using short domain lengths, successfully demonstrating accurate results [38–40]. This confirms that wave modeling can be effectively resolved even at proximity to the object.

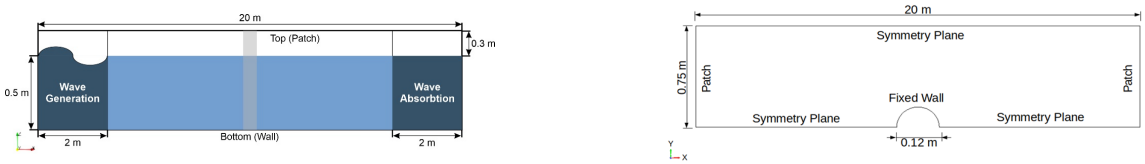

(**a**) (**b**)

Figure 5. (**a**) Computation zone domain on XZ plane. (**b**) Boundary condition on computation domain on XY plane [26].

The simulation encapsulates two scenarios: one characterized by low wave steepness (H = 0.12 m and T = 1.6 s) and another by high wave steepness (H = 0.12 m and T = 1.05 s), both of which are adopted from the study by Devolder, Rauwoens, and Troch [26]. The study focused on CFD of wave-structure interaction simulations to evaluate the effects of different wave steepness conditions on wave dynamics and hydrodynamic loads. The verification model investigates how low-steepness and high-steepness waves impact wave propagation, wave breaking, energy dissipation, and turbulence generation near the structure and hydrodynamic forces exerted on offshore structures.

To accurately simulate fluid dynamics, a modified k-ω SST turbulent model is utilized, enhanced with a buoyancy term. The simulation outcomes and exact calculation findings are briefly outlined in Table 3, showing the body force applied to the monopile structure under varying wave steepness conditions.

Table 3. Body force at monopile structure.

Wave Steepness	Simulation Results	Exact Solution Results	Error (%)
Low (H = 0.12 m and T = 1.6 s)	5.048 N	5.104 N	1.1%
High (H = 0.12 m and T = 1.05 s)	4.448 N	4.459 N	0.25%

The exact solution is derived from the research conducted by Devolder, Rauwoens, and Troch, which were obtained using Richardson's extrapolation method to estimate the force on the monopile at an infinitely fine grid resolution [26]. The analysis indicates that the discrepancy between simulation results and exact calculations remains consistently below 2%. Notably, even under both low and high wave steepness conditions, the difference stays within acceptable thresholds, reinforcing the credibility of the simulation results.

In summary, the validity of the simulation outcomes is confirmed through a comprehensive comparison of simulation data with theoretical calculations across various wave conditions. This validation demonstrates the reliability and accuracy of the simulation framework used in this study.

4.2. Wave Behavior on the Jack-Up Production Platform Hull Structures

A brief grid independence study was conducted to assess mesh sensitivity and ensure that the selected number of cells and mesh topology adequately support the simulation, thereby yielding reliable results. The evaluation was carried out specifically for Case C, characterized by a wave height of 4 meters and a wave period of 5.1 seconds. Three simulation scenarios with different cell counts were analyzed. The horizontal force acting on the structure was selected as the validation parameter, monitored over a 55.5-second period. The results indicate that all models produced comparable horizontal forces, with maximum loads of 132.41 kN, 316.12 kN, and 318.501 kN for the meshes containing 648,465, 1,512,568, and 1,957,004 cells, respectively. As shown in Figure 6, the relative error between the last two scenarios is approximately 0.7%, which is within an acceptable range for engineering simulations. These findings confirm that the model with 1,957,004 cells achieves grid independence, as further refinement has a negligible impact on the simulation outcomes.

Figure 7 illustrates the wave behavior upon collision with the jack-up production platform in Case C (H = 4 m, T = 5.1 s). At t = 56 s, the wave initially impacts the underside of the platform and continues propagating until it reaches the rear side of the platform's bottom at t = 58 s. In Figure 7, the changes in wave characteristics due to interaction with the platform are evident. Unlike unobstructed waves, which maintain their original propagation, waves that collide with the structure experience significant damping, leading

to gradual dissipation over time. This highlights the considerable influence of the platform on wave propagation dynamics.

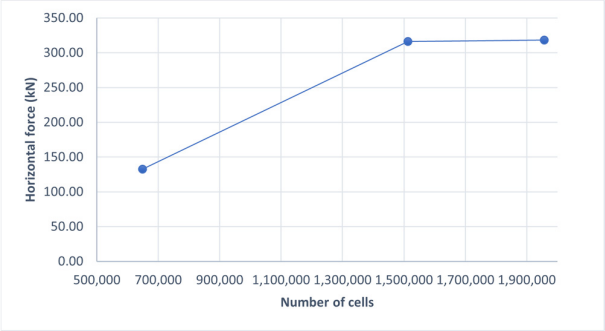

Figure 6. Grid independent result.

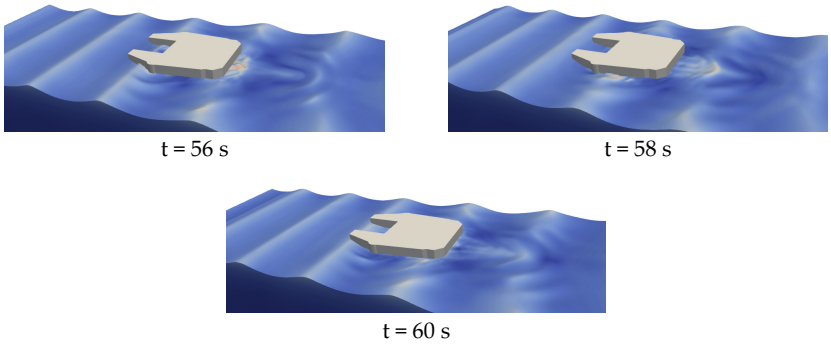

Figure 7. Wave profile on the jack-up production platform structure at three various times from test case C (H = 4 m and T = 5.1 s).

4.3. Wave Loads on Jack-Up Production Platform Structure

Figure 8 presents the graph of the total horizontal force acting on the wall of the jack-up production platform. The total force is computed using a standard surface integral method within the CFD solver, which sums the forces acting on all surface cells of the platform.

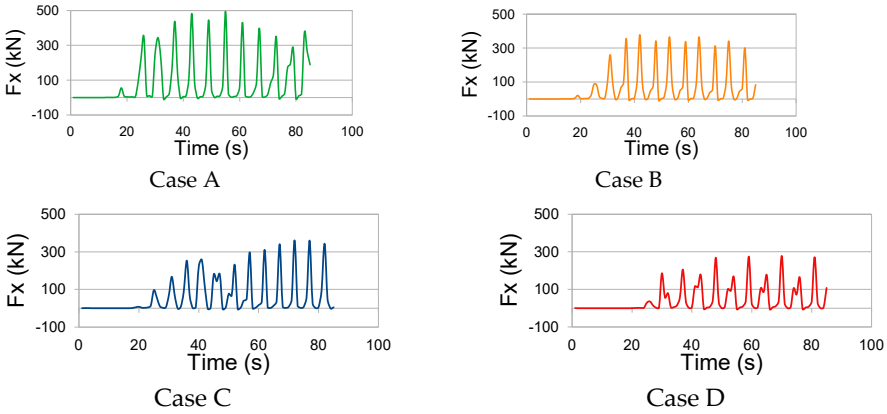

Figure 8. Graph the horizontal forces acting on the jack-up production platform structure with the wave test case variation.

It can be seen in Figure 8 that the total force of all cases fluctuates. This shows that the occurrence load in the platform is not steady and varies in time. In Case D, wave hits the platform with the lowest load and experiences more fluctuations. The load capacity is likely influenced by wave height with Case A having the highest load capacity. Apart

from horizontal load, the platform is also hit by vertical load which is shown in Figure 9. Compared to horizontal load, vertical load has higher capacity.

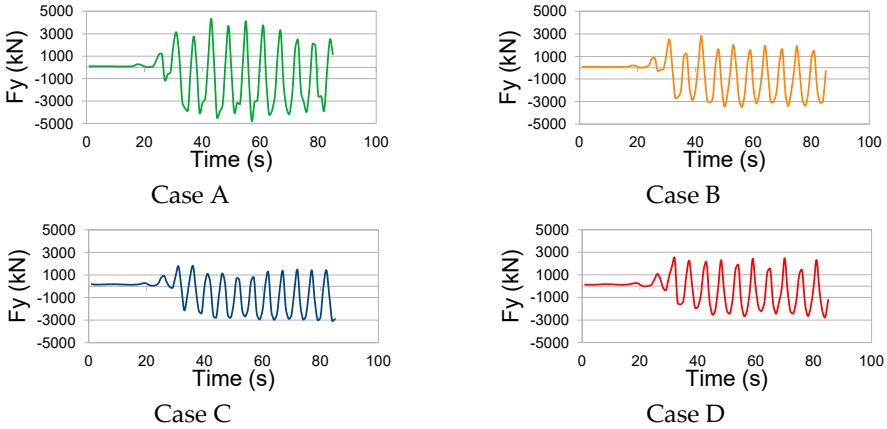

Figure 9. Graph of the vertical forces acting on the jack-up production platform structure with the wave test case variation.

The data presented in Figure 9 reveals significant variability in the vertical force applied to the jack-up production platform structure across different wave test cases. Notably, the peak horizontal force magnitude varies among test scenarios, with the highest observed in test case variation A (H = 5.4 m and T = 5.9 s), reaching around 480 kN, while the lowest is recorded in test case variation D (H = 3.7 m and T = 5.5 s), at approximately 280 kN.

The result shows that the height and period of the waves are directly correlated with the highest force magnitude which is the time-integral of the absolute value of the force on the monopile in X-direction over one wave period when the first wave reaches the outlet boundary [26]. Higher maximum forces result from the expanding impacting water mass on the structure caused by an increase in wave height and period. Furthermore, the force graph shows a secondary peak that can be attributed to the intricate profile of the production platform structure of the jack-up, namely where it meets the wave. Furthermore, wave reflection upon impacting the platform wall is indicated by negative values in the horizontal force direction.

Additionally, Figure 9 illustrates the graph depicting the average vertical force acting on the platform's wall. This aspect offers insights into the vertical forces experienced by the structure, crucial for evaluating its stability and structural integrity under wave loading conditions.

The analysis of horizontal force variations elucidates the intricate dynamics of wave-structure interaction, underscoring the importance of considering wave characteristics such as height and period in assessing structural responses. Furthermore, the representation of vertical force trends provides valuable information for evaluating overall structural performance and ensuring the safety and stability of the jack-up production platform in offshore environments.

The examination of the vertical force graph portrayed in Figure 9 reveals notable disparities in the maximum vertical force among various wave test cases. Particularly, the highest maximum vertical force is evident in test case variation A (H = 5.4 m and T = 5.9 s), peaking at approximately 4000 kN, whereas the lowest maximum vertical force occurs in test case variation D (H = 3.7 m and T = 5.5 s), registering around 2400 kN.

Similarly to the horizontal force findings, the vertical force data showcases a trend where increasing the wave height and period correlates with heightened forces acting on the jack-up production platform structure. However, distinct characteristics in magnitude and direction differentiate the vertical force from its horizontal counterpart. In the vertical

dimension, forces notably escalate, particularly those leading to the negative axis. This discrepancy in force magnitude between vertical and horizontal components predominantly stems from the geometric positioning of the jack-up production platform above the still water level (SWL).

Due to its elevated stance relative to the water surface, the wave load mostly impacts the platform's lower section, resulting in substantially amplified vertical forces compared to the horizontal ones. Furthermore, negative force values emerge, primarily induced by the downward recoil of water mass after colliding with the platform's wall. This occurrence engenders negative pressure zones, as delineated in Figure 10, contributing to the observed negative force values in the vertical direction.

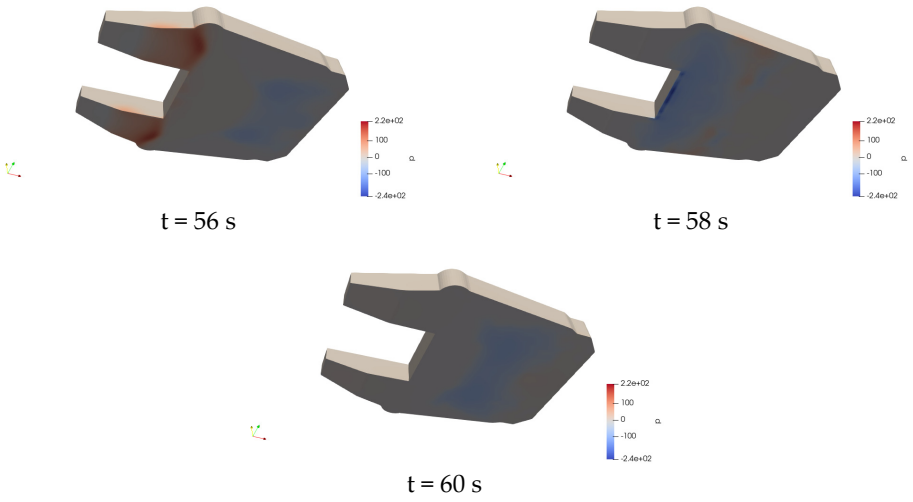

Figure 10. Pressure contour of the waves hiting the wall of the jack-up production platform from test case C (H = 4 m and T = 5.1 s).

The pressure contour on the wall of the jack-up production platform is shown visually in Figure 10, which is in sync with the timing shown in Figure 7. Figure 10 representation of pressure distribution provides important information about the composition and properties of forces operating on the structure.

Looking at Figure 10, it is clear that a significant percentage of pressure values are concentrated in the lower part of the wall of the jack-up production platform. The predominance of vertical forces over horizontal forces is mostly due to this pressure concentration. In particular, positive pressure is applied during the wave's first contact on the platform's bottom wall (at t = 56 s), which causes a vertical force to be directed along the positive axis.

After this first effect, a vacuum effect occurs when the wave recoils towards the bottom of the platform (at t = 58 s and t = 60 s), producing negative pressure. The observed variations in force dynamics are a result of the vertical forces produced by this negative pressure event, which are oriented along the negative axis.

The pressure contour in Figure 10 and the wave-induced forces in Figure 7 are temporally aligned, providing important information about the complex interactions between wave dynamics and structural responses. The observed fluctuations in pressure highlight the complexity of the interactions between waves and structures, as well as the significance of taking into account both the positive and negative pressure effects when assessing the stability and performance of structures in offshore environments.

Furthermore, CFD simulations using the SGDH turbulence model are closely linked to the mechanical integrity of offshore platforms. This connection arises from the wave loads and forces extracted from the simulation, which directly influence the stress–strain deformation of the platform structure. Building upon the successful modeling of hydro-

dynamic loading on jack-up platforms, it is crucial to evaluate the mechanical integrity of these structures under such conditions. This evaluation follows established offshore design standards, which provide guidelines on wave-induced forces, structural strength, and fatigue life. Adhering to these standards ensures that offshore platforms can withstand extreme environmental conditions while maintaining operational safety and reliability.

5. Conclusions

In this study, a Computational Fluid Dynamics (CFD) analysis using OpenFOAM was employed to scrutinize the hydrodynamic load exerted on the jack-up production platform structure. Several key conclusions emerged from this investigation:

- The force load experienced by the jack-up production platform structure correlates directly with the magnitude of wave height and the wave period. Notably, the research identified the maximum wave load in test case A (H = 5.4 m and T = 5.9 s) and the minimum wave load in test case D (H = 3.7 m and T = 5.5 s). As the wave height and period increase, the mass of water impacting the walls of the jack-up production platform amplifies accordingly.
- Due to the geometric positioning of the jack-up production platform above the Still Water Level (SWL), the predominant forces acting on the platform walls manifest predominantly in the vertical direction.
- The study revealed that the vertical force along the negative axis exhibits a significant magnitude, primarily induced by the rebounding of water waves from the jack-up production platform's walls after the initial collision. This phenomenon causes a vacuum effect, generating negative pressure on the bottom wall of the jack-up production platform.

The computed hydrodynamic forces can be further explored in future studies to integrate the hydrodynamic evaluations with the mechanical integrity assessment of the platform. This integration can be validated against offshore design standards, such as the API RP 2A-WSD (Planning, Designing, and Constructing Fixed Offshore Platforms—Working Stress Design) and DNV-OS-C101 (Design of Offshore Steel Structures), ensuring compliance with industry best practices and the established offshore safety criteria. By combining CFD simulations with structural analysis, the results confirm that the platform design meets or exceeds the requirements outlined in offshore standards. This ensures structural resilience under both operational and extreme environmental conditions, enhancing the platform's safety and reliability.

Author Contributions: Conceptualization, N.R.A. and E.C.I.; Methodology, N.R.A., G.M. and E.C.I.; Software, G.M.; Validation, G.M.; Formal analysis, N.R.A., T.H.A. and M.M.-T.; Investigation, G.M. and T.H.A.; Resources, M.M.-T.; Data curation, M.M.-T.; Writing—original draft, G.M.; Writing—review & editing, D.S.; Visualization, E.C.I., T.H.A. and D.S.; Supervision, N.R.A., E.C.I., T.H.A. and M.M.-T.; Project administration, D.S. All authors have read and agreed to the published version of the manuscript.

Funding: This research was funded by Indonesian Ministry of Higher Education, Science, and Technology under 2024 Matching Fund Grant number 2860.

Data Availability Statement: The original contributions presented in this study are included in the article. Further inquiries can be directed to the corresponding author.

Conflicts of Interest: The authors declare no conflict of interest.

Nomenclature

A	Scale ratio
D_ω	Cross diffusion term
g	Gravitational acceleration
F_1, F_2	blending function that helps transition between different turbulence models
G_ω	Generation of ω due to turbulence
G_k	Generation of **k** due to shear in the velocity field
k	Turbulence kinetic energy
L	Length
S	Strain rate magnitude
V	Velocity
Y_k	Rate at which turbulent kinetic energy is converted into thermal energy due to viscosity
Y_ω	Destruction (dissipation) of ω due to viscosity effects.
α	Empirical model constants
β	Model constant
Γ_k	Effective diffusivity for turbulent kinetic energy
Γ_ω	Effective diffusivity of ω
λ_L	Wave length
μ	Viscosity
σ	Turbulence model constant
ω	Turbulence specific dissipation rate
Superscript	
T	Transpose
Superscript	
m	Model scale
p	Real scale
t	Turbulent (turbulent eddy)

References

1. BP. *BP Statistical Review of World Energy*, 68th ed.; BP: London, UK, 2019; Available online: https://www.bp.com/content/dam/bp/business-sites/en/global/corporate/pdfs/energy-economics/statistical-review/bp-stats-review-2019-full-report.pdf (accessed on 24 January 2024).
2. BP. *BP Statistical Review of World Energy*, 72nd ed.; BP: London, UK, 2023; Available online: https://www.bp.com/statisticalreview (accessed on 24 January 2024).
3. Randall, R.E. *Elements of Ocean Engineering*, 2nd ed.; Society of Naval Architects: College Station, TX, USA, 2010.
4. Azman, N.U.; Abu Husain, M.K.; Mohd Zaki, N.I.; Mat Soom, E.; Mukhlas, N.A.; Syed Ahmad, S.Z.A. Structural Integrity of Fixed Offshore Platforms by Incorporating Wave-in-Deck. *J. Mar. Sci. Eng.* **2021**, *9*, 1027. [CrossRef]
5. Ghazi, Z.M.; Abbood, I.S.; Hejazi, F. Dynamic Evaluation of Jack-up Platform Structure under Wave, Wind, Earthquake and Tsunami Loads. *J. Ocean. Eng. Sci.* **2022**, *7*, 41–57. [CrossRef]
6. Kagita, G.; Addala, M.B.; Achary, G.G.S.; Sripada, S.V.R. Evaluation of Impact Loads on Offshore Jacket Platform during Float-over Mating Operation. *Int. Conf. Ocean. Offshore Arct. Eng.* **2019**, *1*, V001T01A013. [CrossRef]
7. Luo-Theilen, X.; Rung, T. Numerical Analysis of the Installation Procedures of Offshore Structures. *Ocean. Eng.* **2019**, *179*, 116–127. [CrossRef]
8. Ye, H.; Yu, D.; Ye, J.; Yang, Z. Numerical Analysis of Dynamics of Jack-Up Offshore Platform and Its Seabed Foundation under Ocean Wave. *Appl. Sci.* **2022**, *12*, 3299. [CrossRef]
9. Tang, W.; Zhuang, H.; Tang, Z.; Guo, S.; Yan, F. Mooring Positioning Performance of Jack-up Platform. *Ships Offshore Struct.* **2020**, *15*, 633–644. [CrossRef]
10. Abdel Raheem, S.E. Nonlinear Behaviour of Steel Fixed Offshore Platform under Environmental Loads. *Ships Offshore Struct.* **2014**, *11*, 1–15. [CrossRef]
11. Xie, Y.; Huang, J.; Li, X.; Tian, X.; Liu, G.; Leng, D. Experimental Study on Hydrodynamic Characteristics of Three Truss-Type Legs of Jack-up Offshore Platform. *Ocean. Eng.* **2021**, *234*, 109305. [CrossRef]
12. Wu, Y.-S. *Multiphase Fluid Flow in Porous and Fractured Reservoirs*; Gulf Professional Publishing: Houston, TX, USA, 2016.

13. Zhou, Y.; Xiao, Q.; Liu, Y.; Incecik, A.; Peyrard, C.; Wan, D.; Pan, G.; Li, S. Exploring Inflow Wind Condition on Floating Offshore Wind Turbine Aerodynamic Characterisation and Platform Motion Prediction Using Blade Resolved CFD Simulation. *Renew. Energy* **2022**, *182*, 1060–1079. [CrossRef]
14. Jiang, S.; Chen, G.; Zhu, Y.; Li, X.; Shen, X.; He, R. Real-Time Risk Assessment of Explosion on Offshore Platform Using Bayesian Network and CFD. *J. Loss Prev. Process Ind.* **2021**, *72*, 104518. [CrossRef]
15. Elhanafi, A.; Macfarlane, G.; Fleming, A.; Leong, Z. Experimental and Numerical Measurements of Wave Forces on a 3D Offshore Stationary OWC Wave Energy Converter. *Ocean. Eng.* **2017**, *144*, 98–117. [CrossRef]
16. Nematollahi, M.; Moghim, M.N. Numerical Simulation of Spatial Distribution of Wave Overtopping on Non-Reshaping Berm Breakwaters. *J. Marine. Sci. Appl.* **2020**, *19*, 301–316. [CrossRef]
17. Cui, F.; Daskiran, C.; King, T.; Robinson, B.; Lee, K.; Katz, J.; Boufadel, M.C. Modeling Oil Dispersion under Breaking Waves. Part I: Wave Hydrodynamics. *Environ. Fluid Mech.* **2020**, *20*, 1527–1551. [CrossRef]
18. Yao, Y.; Chen, X.; Xu, C.; Jia, M.; Jiang, C. Modeling Solitary Wave Transformation and Run-up over Fringing Reefs with Large Bottom Roughness. *Ocean. Eng.* **2020**, *218*, 108208. [CrossRef]
19. Aggarwal, A.; Chella, M.A.; Bihs, H.; Arntsen, Ø.A. Numerical Study of Irregular Breaking Wave Forces on a Monopile for Offshore Wind Turbines. *Energy Procedia* **2017**, *137*, 246–254. [CrossRef]
20. Chella, A.M.; Bihs, H.; Myrhaug, D. Wave Impact Pressure and Kinematics Due to Breaking Wave Impingement on a Monopile. *J. Fluids Struct.* **2019**, *86*, 94–123. [CrossRef]
21. Leftheriotis, G.A.; Chalmoukis, I.A.; Oyarzun, G.; Dimas, A.A. A Hybrid Parallel Numerical Model for Wave-Induced Free-Surface Flow. *Fluids* **2021**, *6*, 350. [CrossRef]
22. Wang, W.; Bihs, H.; Kamath, A.; Arntsen, Ø.A. Multi-Directional Irregular Wave Modelling with CFD. In Proceedings of the Fourth International Conference in Ocean Engineering (ICOE2018); Murali, K., Sriram, V., Samad, A., Saha, N., Eds.; Lecture Notes in Civil Engineering. Springer: Singapore, 2019; Volume 22, pp. 521–529. [CrossRef]
23. Frantzis, C.; Grigoriadis, D.G.E.; Dimas, A.A. Numerical Study of Solitary Waves Past Slotted Breakwaters with a Single Row of Vertical Piles: Wave Processes and Flow Behavior. *Ocean. Eng.* **2020**, *211*, 107667. [CrossRef]
24. Nizamani, M.; Nizamani, Z.; Nakayama, A.; Osman, M. Analysis of Loads Caused by Waves on the Deck near the Free Surface of the Offshore Platform Using Computational Fluid Dynamics. *Ships Offshore Struct.* **2022**, *17*, 1964–1974. [CrossRef]
25. Dong, G.; Gao, X.; Ma, X.; Ma, Y. Energy Properties of Regular Water Waves over Horizontal Bottom with Increasing Nonlinearity. *Ocean. Eng.* **2020**, *218*, 108159. [CrossRef]
26. Devolder, B.; Rauwoens, P.; Troch, P. Application of a Buoyancy-Modified k-ω SST Turbulence Model to Simulate Wave Run-up around a Monopile Subjected to Regular Waves Using OpenFOAM ®®. *Coast. Eng.* **2017**, *125*, 81–94. [CrossRef]
27. Huo, S.; Deng, S.; Song, Z.; Zhao, W.; Wan, D. On the Hydrodynamic Response and Slamming Impact of a Cylindrical FPSO in Combined Wave-Current Flows. *Ocean. Eng.* **2023**, *275*, 114139. [CrossRef]
28. Jacobsen, N.G.; Fuhrman, D.R.; Fredsøe, J. A Wave Generation Toolbox for the Open-source CFD Library: OpenFoam®®. *Numer. Methods Fluids* **2012**, *70*, 1073–1088. [CrossRef]
29. Karola, A.; Tavakoli, S.; Mikkola, T.; Matusiak, J.; Hirdaris, S. The Influence of Wave Modelling on the Motions of Floating Bodies. *Ocean Eng.* **2024**, *306*, 118067. [CrossRef]
30. Brown, S.A.; Greaves, D.M.; Magar, V.; Conley, D.C. Evaluation of Turbulence Closure Models under Spilling and Plunging Breakers in the Surf Zone. *Coast. Eng.* **2016**, *114*, 177–193. [CrossRef]
31. Islam, H.; Guedes Soares, C. Assessment of Uncertainty in the CFD Simulation of the Wave-Induced Loads on a Vertical Cylinder. *Mar. Struct.* **2021**, *80*, 103088. [CrossRef]
32. Bruinsma, N. *Validation and Application of a Fully Nonlinear Numerical Wave Tank*; Delft University of Technology: Delft, The Netherlands, 2016.
33. Sayigh, A. *Comprehensive Renewable Energy*, 1st ed.; Elsevier: Amsterdam, The Netherlands, 2012.
34. Keser, R. *Block-Coupled Solution Algorithms for 2-Equation Turbulence Models*; Fakultet Strojarstva i Brodogradnje: Zagreb, Croatia, 2016; p. 110.
35. Devolder, B.; Troch, P.; Rauwoens, P. Performance of a Buoyancy-Modified k-ω and k-ω SST Turbulence Model for Simulating Wave Breaking under Regular Waves Using OpenFOAM®®. *Coast. Eng.* **2018**, *138*, 49–65. [CrossRef]
36. Kumar, R.; Dewan, A. Assessment of Buoyancy-Corrected Turbulence Models for Thermal Plumes. *Eng. Appl. Comput. Fluid Mech.* **2013**, *7*, 239–249. [CrossRef]
37. Devolder, B. *Hydrodynamic Modelling of Wave Energy Converter Arrays*; KU LEUVEN: Leuven, Belgium, 2018.
38. Jasak, H.; Vukčević, V.; Gatin, I. Numerical Simulation of Wave Loading on Static Offshore Structures. In *CFD for Wind and Tidal Offshore Turbines*; Springer International Publishing: Cham, Switzerland, 2015; pp. 95–105.

39. Liu, B.; Park, S. CFD Simulations of the Effects of Wave and Current on Power Performance of a Horizontal Axis Tidal Stream Turbine. *J. Mar. Sci. Eng.* **2023**, *11*, 425. [CrossRef]
40. Chen, Z.; Jiao, J.; Jiang, C.; Si, H.; Chen, S. Scale Effects on Wave Loads and Slamming Loads in Ship Hydroelasticity Simulation by CFD-FEM Method. *Ocean Eng.* **2024**, *314*, 119718. [CrossRef]